

# Comptonization and QPO Origins in Accreting Neutron Star Systems

Hyong C. Lee<sup>1</sup> and Guy S. Miller<sup>2</sup>

Department of Physics and Astronomy, Northwestern University,  
2145 Sheridan Road, Evanston, IL 60208, USA.

Received \_\_\_\_\_; accepted \_\_\_\_\_

arXiv:astro-ph/9712240v1 17 Dec 1997

---

<sup>1</sup>E-mail: hyongel@nwu.edu

<sup>2</sup>E-mail: gsmiller@casbah.acns.nwu.edu

## ABSTRACT

We develop a simple, time-dependent Comptonization model to probe the origins of spectral variability in accreting neutron star systems. In the model, soft “seed photons” are injected into a corona of hot electrons, where they are Compton upscattered before escaping as hard X-rays. The model describes how the hard X-ray spectrum varies when the properties of either the soft photon source or the Comptonizing medium undergo small oscillations. Observations of the resulting spectral modulations can determine whether the variability is due to (i) oscillations in the injection of seed photons, (ii) oscillations in the coronal electron density, or (iii) oscillations in the coronal energy dissipation rate. Identifying the origin of spectral variability should help clarify how the corona operates and its relation to the accretion disk. It will also help in finding the mechanisms underlying the various quasi-periodic oscillations (QPO) observed in the X-ray outputs of many accreting neutron star and black hole systems. As a sample application of our model, we analyze a kilohertz QPO observed in the atoll source 4U 1608-52. We find that the QPO is driven predominantly by an oscillation in the electron density of the Comptonizing gas.

*Subject headings:* accretion, accretion disks — radiation mechanisms: thermal — stars: neutron — X-rays: stars

## 1. Accretion Disk Coronae

The X-ray spectra of accreting neutron stars and black holes in binary systems typically appear to have at least two components (for recent reviews, see White, Nagase, & Parmar 1995; and Tanaka & Lewin 1995). The soft spectral component resembles blackbody radiation. It is thought to come from optically thick gas in the accretion disk and possibly, in the case of an accreting neutron star, from gas near the stellar surface. The hard spectral component comes from hotter gas that fails to reach thermal equilibrium with its radiation; the radiation intensity falls off with increasing photon energy roughly as a power-law,  $I_E \propto E^{-\alpha}$ , up to a cutoff photon energy  $E_c$  beyond which the intensity drops exponentially. In the most rapidly accreting neutron star systems, the Z-sources, the “hard component” cuts off at energies  $\lesssim 10$  keV and appears at least partially thermalized; the hard component extends to higher energies in the atoll sources, which have lower accretion rates, and in black hole candidate systems. The multicomponent appearance of their X-ray spectra suggests that the accretion flows around these objects may be divided into a minimum of two substructures, one consisting of cooler, dense gas that for convenience we shall call the “disk” component, and a coronal component of hotter, tenuous gas. Observations of rapid variability in X-ray binary systems (see van der Klis 1995 for a review) also support this picture of discrete physical substructures in the accretion flow. Fluctuations in the hard spectral component tend to be much more pronounced than those in the soft component, and to be more weakly correlated with fluctuations in the soft component on short timescales than on longer timescales.

Comptonization has long been recognised as the probable source of the hard spectral component in cosmic X-ray sources (Thorne & Price 1975; Shapiro, Lightman, & Eardley 1976), since it naturally produces high-energy spectra of approximately the right shape, and is the dominant interaction between photons and electrons in hot, tenuous gases. (Here

we do not consider neutron stars with surface magnetic fields  $B_s \gtrsim 10^{12}$  Gauss, as their extremely strong magnetic fields make the physics of their X-ray spectra unlike that of other accreting neutron stars.) The hot gas cools by Compton scattering low-energy “seed photons” to higher energies, and the Compton upscattered photons escape the system as the hard spectral component. The source of the seed photons is unclear at present, and is likely to be different in black hole and neutron star systems. In some models for spectral formation in black hole systems (see, for example, Haardt & Maraschi 1993), soft photons from the optically thick disk seed the Comptonization, but in others (e.g., Narayan, Yi, & Mahadevan 1995) the soft photons are due to cyclotron/synchrotron emission from the hot corona itself. In neutron star systems, cyclotron emission from the neutron star magnetosphere can provide the seed photons, and it is probable that Compton emission from hot magnetospheric gas dominates the hard spectrum (Psaltis, Lamb, & Miller 1995); nevertheless, the disk, magnetospheric boundary layer, and stellar surface also may play important roles. The question of where seed photons come from depends on the geometrical relation between the hot and cold flow substructures, which is poorly known at best. For example, in the case of accretion by a black hole, advection-dominated disk models (see Narayan 1996 and references therein) and the classic Shapiro, Lightman, and Eardley scenario have a cold outer disk which becomes hot and optically thin to absorption within some critical radius, so that the corona occupies the most central regions of the flow, while the cold disk lies beyond it; however, models in which the coronal gas sandwiches the colder disk have also received considerable theoretical development (Liang & Price 1977; Bisnovatyi-Kogan & Blinnikov 1977; and Galeev, Rosner, & Vaiana 1979; more recent studies emphasizing spectral formation include Haardt & Maraschi 1993; Haardt, Maraschi, & Ghisellini 1997; and Dove, Wilms, & Begelman 1997). Given the uncertainties, even very general information about the coronal structure and soft photon source would be welcome, in black hole candidate and in neutron star systems.

Rapid X-ray variability is now thought to hold vital clues to the nature of the accretion flow “engines” in these systems. In particular, quasi-periodic oscillations have attracted attention from both observers and theorists, since they are believed to contain otherwise inaccessible information about the structure and operation of the central accretion flow. (A quasi-periodic oscillation, or QPO, is enhanced variability in a relatively narrow range of frequencies around a so-called “centroid” or QPO frequency, which thus resembles but is not identical to periodic modulation in the emission from a source.) The QPO so far discovered in X-ray binaries span a wide range of frequencies, from  $\nu_{\text{QPO}} \lesssim 1$  Hz to over a kilohertz, and appear to belong to a number of phenomenologically distinct categories, each of which presumably has a different mechanism. Proposed mechanisms for QPO tend to be situated within or near the radiation-generating central regions of their accretion flows, and include modulations of the flow at the inner edge of the disk or at the magnetospheric boundary (for the classic “magnetospheric beat frequency” models, see Alpar & Shaham 1985, and Lamb et al. 1985; also see Miller, Lamb, & Psaltis 1997 for a beat frequency model applied to the recently discovered kilohertz QPO), wave-like oscillations in the inner disk (e.g., Chen & Taam 1995, and references therein), and oscillations in a coronal flow component (Fortner, Lamb, & Miller 1989; Miller & Lamb 1992). Although leading candidate models have emerged for one or two of the QPO categories, satisfactory explanations exist for very little of the rich QPO phenomenology that has come to light over the past decade. QPO remain promising, and enigmatic.

Without assuming a detailed hydrodynamic model for the QPO, several attempts have been made to extract general information about the physical characteristics of the accretion flow and the QPO mechanism from the spectral structure of the observed QPO; i.e., how the amplitude of the QPO varies from one band of photon energies to the next, and the degree to which the oscillation in a given band lags behind those in other bands. Early EXOSAT-based studies of the 20–50 Hz QPO in Z-sources (Hasinger 1987, van der

Klis 1987) showed that X-ray photons at higher energies lag behind those at lower energies by several milliseconds, an effect which immediately suggested the progression of photons from lower to higher energies in a Comptonizing corona. The discovery stimulated several groups to perform calculations of time-dependent Comptonization in which the soft photon injection rate underwent small oscillations about its average value (Wijers, van Paradijs, & Lewin 1987; Stollman et al. 1987). In addition to injection rate oscillations, Stollman et al. (1987) examined the effects of small oscillations in the coronal electron density. They concluded that either type of modulation, in the soft photon source or in the coronal electron density, could account for the observed hard lag; the data available at the time were insufficient to discriminate between the two possibilities.

Observations of accreting neutron star and black hole binary systems with the Rossi X-ray Timing Explorer (RXTE) satellite have revealed unprecedented detail in their X-ray variations, and motivate us to return to the issue of how much can be learned about X-ray coronae and the origins of X-ray variability through time-dependent Comptonization models. In this paper we develop a method of calculating spectral variations based on the time-dependent Kompaneets equation that is far more computationally efficient than the Monte Carlo methods employed by Wijers et al. and Stollman et al. Our calculations permit us to introduce small oscillations into *any* of the underlying properties of the Comptonization process and study how they drive the emerging radiation. Since the Kompaneets approach is best for systems with scattering optical depths  $\tau$  well above unity, our method is more appropriate for accreting neutron star systems (in which coronal optical depths are expected to be  $\gtrsim 5$ ) than for black hole candidate systems (in which it is estimated  $\tau \lesssim 1$ ). Using values for coronal parameters expected to be characteristic of neutron star systems, we explore how X-ray spectral variations depend on coronal properties and on the nature of the underlying driving modulation. We show that considerable differences exist between the spectral variations produced by modulations in the soft photon

injection, in the coronal electron density, and in the coronal electron temperature. These differences should make it possible to fit observed spectral variations as a superposition of the different types of modulation, and to obtain constraints on QPO mechanisms and on system parameters such as the size of the Comptonizing corona that are more reliable than those obtained by considering only one type of modulation in isolation.

## 2. Time-dependent Comptonization Model

Since the properties of an accretion disk corona and its soft photon source are so poorly known, we adopt the simplest possible description for them consistent with our goal of physically interpreting variability in hard X-ray spectra. We ignore the effects of gradients in the electron density and temperature of the corona, and treat the Comptonization process as if it occurred in a completely homogeneous medium with electron density  $n_e$  and temperature  $T$ . We do, however, allow these quantities to undergo small oscillations as photons in the corona are Comptonized. We further enforce the assumption that the corona is homogeneous by stipulating that once injected into the corona, any photon may escape from it with a probability per unit time

$$\Gamma_{\text{esc}} = c\sigma_T n_e / N_{\text{esc}} \equiv 1 / (N_{\text{esc}} t_c), \quad (1)$$

where  $c$  is the speed of light and  $\sigma_T$  is the Thomson cross section. The escape rate  $\Gamma_{\text{esc}}$  depends only on the mean time between collisions,  $t_c$ , and on the average number  $N_{\text{esc}}$  of collisions suffered by a photon before its escape. Thus the model omits any information about the location of a photon within the corona, and all of the properties of the corona are subsumed in the three quantities,  $T$ ,  $t_c$ , and  $N_{\text{esc}}$ .

Our model also treats the injected photons simply. Photons enter the Comptonizing environment at a rate  $\dot{N}$ . At the instant of its entry, the probability that a photon has an

energy between  $E$  and  $E + \delta E$  is given by  $f_{\text{inj}}(E)\delta E$ . In this paper, we will take the injected photon distribution to have a blackbody spectrum:  $f_{\text{inj}}(E) = AT_{\text{inj}}^{-3}E^2(\exp[E/T_{\text{inj}}] - 1)^{-1}$ , where  $A$  is a normalisation constant. (We write the temperature in units of energy, so that Boltzmann's constant  $k_B \equiv 1$ .) To study how fluctuations in the injection process influence the spectrum of photons escaping from the corona, we introduce small oscillations in  $\dot{N}$  about its average value. We do not permit  $f_{\text{inj}}$  to vary. Thus, we allow for variability in the overall rate of photon injection, but ignore more subtle modulations in the injected spectrum.

For nonrelativistic coronal temperatures ( $T \ll m_e c^2$ ) and sufficiently low photon energies ( $E \ll m_e c^2$ ), the Kompaneets equation (Kompaneets 1957; see Psaltis and Lamb 1997 for a complete derivation of the equation and a discussion of its limitations),

$$t_c \partial_t f = \frac{1}{m_e c^2} \partial_E \left[ -4TEf + E^2 f + T \partial_E (E^2 f) \right] + t_c \dot{N} f_{\text{inj}} - \frac{f}{N_{\text{esc}}}, \quad (2)$$

describes the temporal development of the distribution  $f$  of photons in the Comptonizing medium. The Kompaneets equation is essentially a photon continuity equation in energy. Its natural boundary conditions are that the term in square brackets (the photon current) vanish as  $E \rightarrow 0$  and as  $E \rightarrow \infty$ .

The spectrum of photons escaping from the Comptonizing medium is given by

$$f_{\text{out}}(E) \equiv \Gamma_{\text{esc}} f, \quad (3)$$

so that modulations in the observed spectrum can be driven both by changes in the spectrum  $f$  of photons within the cloud and by changes in the rate  $\Gamma_{\text{esc}}$  at which photons escape from the cloud.

To find how variations in the Comptonization process affect the escaping spectrum, we assume that a given parameter in our model executes small oscillations around its average value, and solve for the resulting behavior of the escaping spectrum to first order in the



oscillating perturbation. For example, to see how  $f_{\text{out}}$  reacts to variations in the photon injection rate  $\dot{N}$ , we would write the injection rate as the sum of a constant value  $\dot{N}_0$  and a small oscillatory part:

$$\dot{N} = \dot{N}_0 + \dot{N}_1 e^{-i\omega t}. \quad (4)$$

Then to first order in the perturbation, the escaping photon spectrum is given by

$$f_{\text{out}}(E) \approx f_{\text{out}0} + e^{-i\omega t} f_{\text{out}1}; \quad (5)$$

where  $f_{\text{out}0}$  is the escaping spectrum in the limit of a vanishing perturbation,

$$f_{\text{out}1} = f_1 / [t_c N_{\text{esc}}]_0, \quad (6)$$

and the perturbation amplitude  $f_1$  of the coronal spectrum is given by the linearised Kompaneets equation,

$$\left( \frac{1}{N_{\text{esc}}} - i\omega t_c \right) f_1 + \frac{1}{m_e c^2} \frac{d}{dE} \left[ 4TE f_1 - E^2 f_1 - T \frac{d}{dE} E^2 f_1 \right] = t_c f_{\text{inj}} \dot{N}_1. \quad (7)$$

In addition to perturbations in the soft photon input, we also consider two types of perturbation in the corona itself. Perturbations in the rate of energy dissipation in the corona drive variations in its temperature:

$$T = T_0 + T_1 e^{-i\omega t}. \quad (8)$$

The escaping photon spectrum is still given by eq. (6), but  $f_1$  is now determined by

$$\left( \frac{1}{N_{\text{esc}}} - i\omega t_c \right) f_1 = \frac{1}{m_e c^2} \frac{d}{dE} \left[ -4E (T_1 f_0 + T_0 f_1) + E^2 f_1 + \frac{d}{dE} E^2 (T_1 f_0 + T_0 f_1) \right]. \quad (9)$$

Perturbations in the supply of matter to the corona can cause its size  $l$  or electron density  $n_e$  to change, altering  $t_c$  and  $N_{\text{esc}}$ . We assume that  $N_{\text{esc}}$  is connected to the electron density  $n_e$  through  $N_{\text{esc}} = \tau(\tau + 1)$ , where the scattering optical depth of the corona is defined to be  $\tau \equiv \sigma_T n_e l$ . Thus,

$$t_c = \frac{l}{c\tau} = \frac{2l}{c} \left( [4N_{\text{esc}} + 1]^{1/2} - 1 \right)^{-1}. \quad (10)$$

(This choice is motivated by simplicity; the exact form of the relationship between  $N_{\text{esc}}$  and  $t_c$  or  $n_e$  depends on geometrical assumptions, and on how the length scale  $l$  is defined. As an example, for escape from the center of a homogeneous Comptonizing sphere, one finds  $N_{\text{esc}} = 3\pi^{-2}\tau[\tau + (4/3)]$  when  $l$  is defined as the radius  $R$  of the sphere, but if one instead defines  $l \equiv 3^{1/2}\pi^{-1}R \approx 0.6R$ , the result is a relationship between  $N_{\text{esc}}$  and  $t_c$  close to the one we assume.) Now the variation in the escaping photon spectrum is given by

$$f_{\text{out}1} = -f_{\text{out}0} \left( \frac{N_{\text{esc}1}}{N_{\text{esc}0}} + \frac{t_{c1}}{t_{c0}} \right) + f_1/[t_c N_{\text{esc}}]_0, \quad (11)$$

where

$$\left( \frac{1}{N_{\text{esc}0}} - i\omega t_{c0} \right) f_1 + \frac{1}{m_e c^2} \frac{d}{dE} \left[ 4TEf_1 - E^2 f_1 - T \frac{d}{dE} E^2 f_1 \right] = \dot{N} f_{\text{inj}t_{c1}} + f_0 \frac{N_{\text{esc}1}}{N_{\text{esc}0}^2} \quad (12)$$

governs the perturbation in the coronal spectrum. Although in general we could allow the parameters  $t_c$  and  $N_{\text{esc}}$  to vary independently, in this paper we will assume that the length scale  $l$  of the corona remains fixed (we choose  $l = 10^6$  cm as characteristic of circumstellar regions in neutron star systems), while the electron density undergoes small oscillations.

This simple model for dynamic Comptonization allows us to study the different spectral variabilities that arise from modulations in the supply of coolant (the soft photons), the supply of heat, and the supply of matter to the corona. In the following section we will examine the characteristics of each type of variability, paying special attention to traits that might serve to distinguish one from another observationally.

### 3. X-ray Variability: Numerical Results

Each type of perturbation — in photon injection, in coronal heating, and in the electron density of the corona — produces a different characteristic variation in the spectrum of the escaping radiation. By identifying the superposition of perturbations that best matches the

observed spectral variations of a given source, we can learn more about the physics of X-ray coronae, and in particular about their sources of material and energy. In this section we solve numerically for the observable spectral variations produced by each of the basic types of perturbation under a range of conditions. We find that, as functions of photon energy, the rms relative amplitude

$$\xi(E) \equiv \frac{1}{\sqrt{2}} \frac{|f_{\text{out}1}|}{f_{\text{out}0}} \quad (13)$$

and the phase

$$\theta(E) \equiv \arctan \left( \frac{\text{Im } f_{\text{out}1}}{\text{Re } f_{\text{out}1}} \right) \quad (14)$$

of each type of spectral variation differ considerably from the other types, and so should be readily distinguishable.

We illustrate the main differences between the three types of spectral variability with a typical model corona. Coronal electrons with an average temperature of  $T_0 = 10 \text{ keV}$  Comptonize 0.1 keV seed photons. The photons suffer on average  $N_{\text{esc}0} = 100$  collisions before escaping from the corona. All the perturbations have frequencies  $\nu = \omega/(2\pi) = 40 \text{ Hz}$  and relative amplitudes of  $10^{-2}$ ; i.e.,  $\dot{N}_1/\dot{N}_0 = 10^{-2}$ ,  $T_1/T_0 = 10^{-2}$ , and  $N_{\text{esc}1}/N_{\text{esc}0} = 10^{-2}$ .

Figure 1 shows the relative amplitudes  $\xi(E)$  (bold lines) and phases  $\theta(E)$  (lighter lines) produced by each perturbation. Oscillations in the seed photon injection rate  $\dot{N}$  cause spectral variations with an approximately energy-independent relative amplitude (bold short dashes); since the residence time of photons in the corona,  $t_{\text{esc}} = 1/\Gamma_{\text{esc}}$ , is short compared to the oscillation period, the spectral response is quasi-static. To a good approximation, the emergent spectrum simply rises and falls with the photon injection rate. The phase lag (light short dashes) is small and has a minimum near the seed injection energy  $T_{\text{inj}}$ ; it rises monotonically with energy above  $T_{\text{inj}}$ . The phase lag corresponds roughly to the time delay  $\sim t_c(m_e c^2/T)$  required by photons to upscatter from low energies  $\sim T_{\text{inj}}$  to higher energies  $\sim T_0$  (as may be estimated from the Kompaneets equation [2]; also see Pozdnyakov,

Sobol, & Sunyaev 1983). Temperature-driven spectral variations (solid lines) are very different. They have a minimum at photon energies near  $3T_0$  and rise sharply thereafter. The associated phase variations also contrast strongly with those due to oscillations in the photon injection rate, and reflect the redistribution of photons from energies below  $\sim 3T_0$  to higher energies that occurs when the coronal temperature increases. Oscillations in the corona’s optical depth (long dashes) alternately overpopulate and depopulate the photon spectrum above  $T_0$ , resulting in a relative amplitude that rises with photon energy near and above  $T_0$ , but less steeply than one driven by coronal temperature oscillations. The spectrum below  $\sim T_0$  falls as the optical depth rises. Oscillations at energies above  $T_0$  are nearly out of phase with those below, except for a phase lag that is caused by the upscattering time delay. Thus, each type of oscillation has its own distinctive signature.

In the following subsections, we systematically examine how each of the spectral oscillation signatures depends on the frequency of the oscillation, and on the average properties of the Comptonizing medium and soft photon injection process. The perturbed spectra depend most strongly on the mean coronal electron temperature  $T_0$ , and on the ratio of the photon residence time to the oscillation period,  $\nu t_{\text{esc}}$ . We choose  $T_0$  to be 5, 10, or 15 keV, characteristic of coronae in accreting neutron star systems. Injection energies  $T_{\text{inj}}$  are drawn from the set {0.1 keV, 0.5 keV, 1 keV}. Oscillation frequencies of  $\nu = 40, 100,$  and 1000 Hz are used to generate the perturbed spectra. Escaping photons experience an average of  $N_{\text{esc}0} = 10, 100,$  and 400 collisions in our calculations, so that the combination  $\nu t_{\text{esc}}$  ranges from  $\sim 10^{-3}$ – $10^0$ , and the spectral response goes from the quasi-static limit to fully dynamic behavior.

### 3.1. Perturbations in the Photon Injection Rate

Suppose that the soft photon source oscillates slightly, driving small oscillations in the emergent spectrum. If the oscillation frequency  $\nu$  is small,  $\nu t_{\text{esc}} \ll 1$ , the response of the spectrum is close to the quasi-static ( $\nu \rightarrow 0$ ) limit. Thus, at all but the highest frequencies, injection modulations simply cause the brightness of the source to undergo small oscillations about its average value, with little change in spectral shape. The relative amplitude is therefore flat, and the phase shifts are small (see Figs. 2a and 2b). Spectral oscillations at higher  $\nu$  have larger phase lags and are more strongly attenuated at energies away from  $T_{\text{inj}}$ .

The dependence of the perturbed spectrum on the coronal temperature  $T_0$  is illustrated in Fig. 2c. The relative amplitude varies little with changes in  $T_0$ . Because the diffusion of photons in energy progresses more rapidly in a hotter corona, the phase lags of the spectral variations are smaller for a hotter corona than for a cooler one. Figure 2d shows that the amplitude of the spectral oscillations above 1 keV has almost no dependence on the injection temperature. The phase lags are somewhat more sensitive to  $T_{\text{inj}}$ , although the dependence is still not strong (approximately logarithmic in  $T_0/T_{\text{inj}}$ ). The phase delay is minimised at energies near  $T_{\text{inj}}$ , since photons escaping at energies near  $T_{\text{inj}}$  typically have spent less time in the corona than photons at more distant energies.

### 3.2. Perturbations in Electron Temperature

Oscillations in the coronal electron temperature force photons from lower to higher energies. The spectral oscillations are thus anticorrelated with the temperature oscillations at low energies, and correlated at higher energies (Fig. 3a). The energy at which the behavior changes from anticorrelation to correlation corresponds to a minimum in the relative amplitude.

When the Comptonized spectrum is very nonthermal (i.e., when the “y-parameter”  $y \equiv 4N_{\text{esc}0}T_0/(mc^2) \ll 1$ ; see Pozdnyakov et al. 1983), the minimum occurs at energies somewhat above  $T_{\text{inj}}$ , but considerably lower than  $T_0$ . Fig. 3b shows that the minimum moves toward an asymptotic position at  $3T_0$  in the case of more thermalized spectra, for which the Wien peak at  $2T_0$  is more prominent (these correspond to  $y \gg 1$ ). This follows from the fact that in the neighborhood of the Wien peak, we expect the time-averaged spectrum to be  $f_0 \approx c_{\text{norm}}E^2T_0^{-3}e^{-E/T_0}$ , where  $c_{\text{norm}}$  is a normalisation constant independent of  $T_0$ . The  $T_0$ -dependence follows from the shape of the thermal peak, and the need to maintain a constant photon number (constant normalisation) at different electron temperatures. In the quasi-static limit the relative spectral variation is then  $T_1e^{-i\omega t}d \ln f_0/dT_0$ , and so the relative amplitude is  $\xi \approx |(-3/T_0 + E/T_0^2)T_1|$ . The approach to the quasi-static, thermalized limit is seen in Fig. 3c. The minimum in the relative amplitude occurs at 6 keV  $\approx 1.2T_0$  for the relatively unthermalized case  $T_0 = 5$  keV, and has reached 33 keV  $\approx 2.2T_0$  in the more thermalized case  $T_0 = 15$  keV.

As Fig. 3d shows, the influence of the photon injection temperature on the spectral oscillations is minor. It is slightly easier for photons introduced at higher energies to form a Wien peak, all other things being equal. Consequently, cases with higher  $T_{\text{inj}}$  are a little better thermalized than cases with lower  $T_{\text{inj}}$ , and have amplitude minima at slightly higher energies.

### 3.3. Perturbations in Electron Density

When the coronal electron density oscillates, the spectral variations at energies near  $T_{\text{inj}}$  are nearly anticorrelated with the driving oscillations. The anticorrelation occurs because an increase in optical depth both suppresses the rate at which photons escape from the cloud and allows photons to evolve to energies more distant from  $T_{\text{inj}}$ . The latter effect

is dominant at energies  $E \gtrsim T_0$ , where the spectral oscillation is nearly in phase with the electron density oscillation, except for a small phase lag due mainly to the time required for photons to diffuse out of the corona.

The dependence of the spectral variations on driving frequency is shown in Fig. 4a. Unsurprisingly, the relative amplitudes of the variations only begin to betray their frequency dependence when the oscillations are fastest, and the spectral response emerges from the quasi-static limit. Since the time lag between the responses in different energy channels has little dependence on the frequency of the driving oscillations in the quasi-static limit, the phase lag at a high photon energies grows approximately linearly with frequency. As the mean electron density increases, the time lag increases, along with the escape time  $t_{\text{esc}}$ . This is seen in the phase lags of Fig. 4b.

Figure 4c shows how the spectral oscillations depend on the mean coronal electron temperature. As one would expect, the minimum in the relative amplitude, which corresponds to the point where the spectral oscillations go from their low-energy anticorrelation with the coronal density oscillations to their high-energy correlation, increases with coronal temperature. When  $T_{\text{inj}}$  is increased, both the phase lag and relative amplitude curves shift upward slightly in energy (Fig. 4d).

#### 4. Preliminary Application to KiloHertz QPO

To illustrate how time-dependent Comptonization calculations can be utilised in data interpretation, we present an informal analysis of an 850 Hz QPO in 4U 1608-52, based on published observations of the energy-dependent QPO phase (Vaughan et al. 1997) and relative amplitude (Berger et al. 1996). With the assumption that oscillations in the soft photon source drive the QPO, Vaughan et al. estimated from the observed phase lags that

the size scale of the coronal gas is between a few kilometers and a few tens of kilometers.

We model the observed spectral variability as a superposition of “basis variabilities” driven by oscillations (i) in the soft photon source, (ii) in the electron density of the Comptonizing corona, and (iii) in the temperature of the coronal electrons. This approach allows the possibility that the energy dependence of the observed oscillation phase might derive from the underlying phase relationships of the basis variabilities and their different energy dependences. For example, a photon injection oscillation might combine with small temperature oscillation that lags it by a quarter cycle. Since the size of the temperature-induced spectral oscillation grows with increasing photon energy, the resulting spectrum would have phase lags that increase steeply with energy, but are unrelated to the time it takes for photons to propagate from lower to higher energies. To safely interpret the phase lags, one should account consistently for the relative amplitude data and the time-averaged spectrum. It is also important that coronal emission dominates the spectral range under consideration. Contamination by (steady) noncoronal emission will reduce the relative amplitude at low photon energies below the model’s predictions.

Since time-averaged spectra for 4U 1608-52 during the QPO observations are not yet publicly available, the coronal parameters we derive must be taken as preliminary, subject to future revision. For example, we found that acceptable fits to the QPO observations could be produced with a wide range of coronal temperatures  $T_0$ . Here, for purposes of illustration, we assumed a temperature  $T_0 = 10$  keV, and an injection spectrum with  $T_{\text{inj}0} = 0.1$  keV. We adjusted the remaining parameters by hand until an acceptable fit was obtained. Our “best fit” appears in Fig. 5. The coronal parameters for the fit are:  $l = 6$  km and  $N_{\text{esc}0} = 20$  (or equivalently,  $\tau = 4$ ). The composition of the driving perturbation is  $n_{e1}/n_{e0} = 0.32$ ,  $\dot{N}_1/\dot{N}_0 = -0.5n_{e1}/n_{e0}$ , and  $T_1/T_0 = -(0.37 + 0.08i)n_{e1}/n_{e0}$ . Although there is considerable latitude in acceptable admixtures of the injection and temperature



perturbations, we found that *to successfully match the relative amplitude data, the primary source of the QPO has to be an oscillation in the coronal electron density. Oscillations dominated by injection or coronal temperature oscillations produce unacceptable fits, even at the qualitative level.*

## 5. Conclusions

Since the spectral variations driven by oscillations in the corona’s supply of soft photons, heat, and material each bear their own distinctive characteristics, one can determine the nature of the oscillations driving QPO. Our sample application to a kilohertz QPO observed in 4U 1608-52 indicates that the main driver behind the QPO is an oscillation in coronal electron density. In agreement with earlier studies (Vaughan et al. 1997), we find that the size of the corona is comparable to estimates of the neutron star radius, supporting the notion that kilohertz QPO originate very close to the accreting neutron star.

This work was supported in part by NASA grants NAGW-2935 and NAG5-3396.

## REFERENCES

- Alpar, M. A., & Shaham, J. 1985, *Nature*, 316, 239
- Lamb, F. K., Shibazaki, N., Alpar, M. A., & Shaham, J. 1985, *Nature*, 317, 681
- Berger, M., van der Klis, M., van Paradijs, J., Lewin, W. H. G., Lamb, F. K., Vaughan, B., Kuulkers, E., Augusteijn, T., Zhang, W., Marshall, F. E., Swank, J. H., Lapidus, I., Lochner, J. C., and Strohmeyer, T. E. 1996, *ApJ*, 469, L13
- Bisnovatyi-Kogan, G. S., & Blinnikov, S. I. 1977, *A&A*, 59, 111
- Chen, X., & Taam, R. E. 1995, *ApJ*, 441, 354
- Dove, J. B., Wilms, J., & Begelman, M. C. 1997, *ApJ*, *in press*
- Fortner, B. F., Lamb, F. K., & Miller, G. S. 1989, *Nature*, 342, 775
- Galeev, A. A., Rosner, R., & Vaiana, G. S. 1979, *ApJ*, 229, 318
- Haardt. F., & Maraschi, L. 1993, *ApJ*, 413, 507
- Haardt. F., Maraschi, L., & Ghisellini, G. 1997, *ApJ*, 476, 620
- Hasinger, G. 1987, in “The Origin and Evolution of Neutron Stars” (IAU Symp. 125), Eds. D. J. Helfand & J. H. Huang (Dordrecht: Reidel), p. 333
- Kompaneets, A. S. 1957, *Sov. Phys.-JETP*, 4, 730
- Liang, E. P. T., & Price, R. H. 1977, *ApJ*, 218, 247
- Miller, G. S., & Lamb, F. K. 1992, *ApJ*, 388, 541
- Miller, M. C., Lamb, F. K., & Psaltis, D. 1997, *ApJ*, submitted
- Narayan, R. 1996, *ApJ*, 462, 136

- Narayan, R., Yi, I., & Mahadevan, R. 1995, *Nature*, 374, 623
- Pozdnyakov, L. A., Sobol, I. M., & Sunyaev, R. A. 1983, *Space Sci. Rev.*, 2, 189
- Psaltis, D., & Lamb, F. K. 1997, *ApJ*, 488, 881
- Psaltis, D., Lamb, F. K., & Miller, G. S. 1995, *ApJ*, 454, L137
- Shapiro, S. L., Lightman, A. P., & Eardley, D. M. 1976, *ApJ*, 204, 187
- Stollman, G. M, Hasinger, G., Lewin, W. H. G., van der Klis, M., & van Paradijs, J. 1987  
*MNRAS*, 227, 7P
- Tanaka, Y., & Lewin, W. H. G. 1995, in “X-ray Binaries”, Eds. W. H. G. Lewin, J. van  
Paradijs, & E. P. J. van den Heuvel (Cambridge: Cambridge Univ. Press), p. 126
- Thorne, K. S., & Price, R. H. 1975, *ApJ*, 195, L101
- van der Klis, M. 1995, in “X-ray Binaries”, Eds. W. H. G. Lewin, J. Van Paradijs, &  
E. P. J. Van den Heuvel (Cambridge: Cambridge University Press), p. 252
- van der Klis, M., Hasinger, G., Stella, L., Langmeier, A., van Paradijs, J., & Lewin,  
W. H. G. 1987, *ApJ*, 319, L13
- Vaughan, B. A., van der Klis, M., Méndez, M., van Paradijs, J., Wijnands, R. A. D., Lewin,  
W. H. G., Lamb, F. K., Psaltis, D., Kuulkers, E., & Oosterbroek, T. 1997 *ApJ*, 483,  
L115
- White, N. E., Nagase, F., & Parmer, A. N. 1995 in “X-ray Binaries”, Eds. W. H. G. Lewin,  
J. Van Paradijs, & E. P. J. Van den Heuvel (Cambridge: Cambridge University  
Press), p. 1
- Wijers, R. A. M. J., van Paradijs, J., & Lewin, W. H. G. 1987, *MNRAS*, 228, 17P



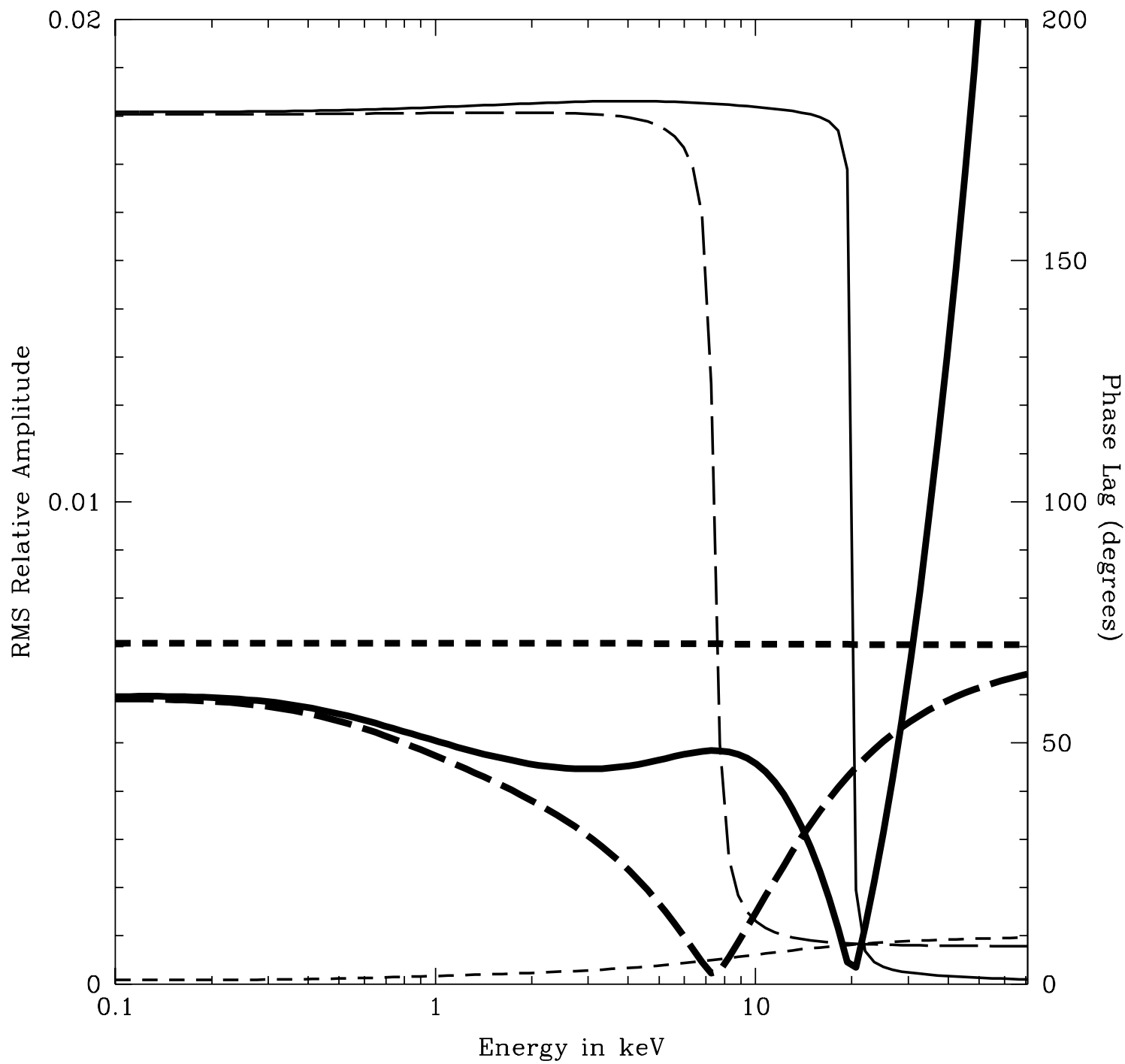
Fig. 1.— When the Comptonization process is disturbed in different ways, distinctive patterns of spectral variability result. Shown are the spectral variations driven by 1% oscillations in (i) the soft photon injection rate (short dashed curves), (ii) the coronal electron temperature (unbroken curves), and (iii) the coronal electron density (long dashed curves). The driving oscillations are all at 40 Hz. Bold lines show the rms relative amplitudes of the spectral oscillations as functions of photon energy. An rms relative amplitude of 1% corresponds to a 1% oscillation in photon count rate about its average value. Light lines show the phase lag between the spectral oscillation and the physical oscillation driving it. Each spectral variation is produced in a “standard” corona with the following time-averaged parameters:  $N_{\text{esc}0} = 100$ ,  $T_{\text{inj}} = 0.1$  keV,  $T_e = 10$  keV, and  $l_{\text{size}} = 10^6$  cm.

Fig. 2.— Spectral variations driven by 1% oscillations in the photon injection rate are illustrated in Figs. 2a–2d. For each variation, a heavy curve denotes the relative amplitude of the spectral oscillation, while the phase lag is depicted by a light curve. Each panel shows how the spectral variations depend on a particular parameter (the oscillation frequency, the average number of collisions suffered by an escaping photon, the coronal temperature, or the temperature of the injected photons), while the other parameters are kept at the values employed in Fig. 1. Fig. 2a compares the spectral responses at different driving oscillation frequencies. Variations induced by photon injection oscillations with frequencies of 40 Hz (unbroken curves), 100 Hz (short dashed curves), and 1 kHz (long dashed curves) are shown. Fig. 2b displays variations in the output spectra of coronae having  $N_{\text{esc}0} = 10$  (short dashed curves), 100 (unbroken curves), and 400 (long dashed curves). Fig. 2c shows variations in the output spectra of coronae with electron temperatures of 5 keV (short dashed curves), 10 keV (unbroken curves), and 15 keV (long dashed curves). Fig. 2d contains spectral variations with several different input photon temperatures: 0.1 keV (unbroken curves), 0.5 keV (short dashed curves), and 1 keV (long dashed curves).

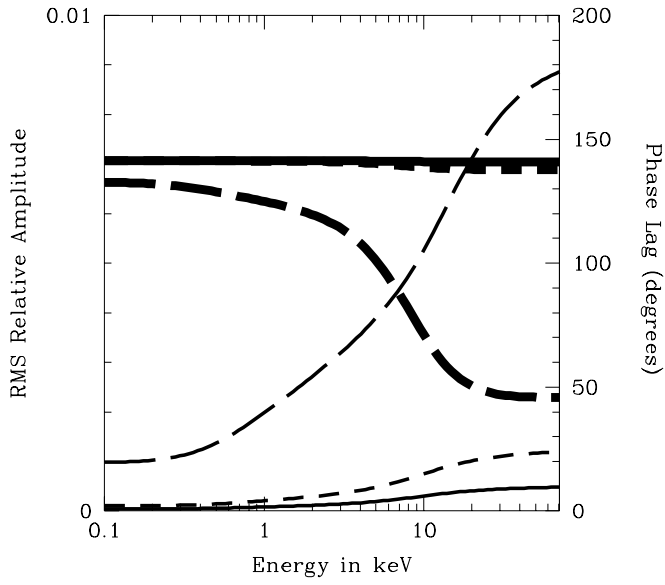
Fig. 3.— Spectral variations driven by 1% oscillations in the coronal temperature. As in Fig. 2, each panel shows how the spectral oscillations depend on the underlying physical properties of the Comptonizing corona and its supply of soft photons.

Fig. 4.— Spectral variations driven by 1% oscillations in the coronal electron density. Each panel shows how the spectral oscillations depend on the underlying physical properties of the Comptonizing corona and its supply of soft photons. The plotting conventions are the same as in Fig. 2.

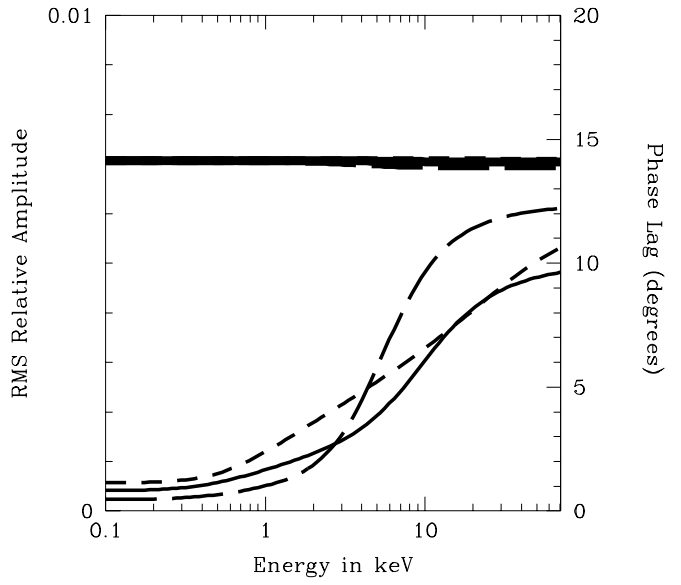
Fig. 5.— Sample fit to an 850 Hz QPO observed in 4U 1608-52. The data for the relative amplitudes are from Berger et al. 1996, and the phase data are from Vaughan et al. 1997. The relative amplitude data imply that the QPO is caused mainly by an oscillation in the coronal electron density, rather than by oscillations in the soft photon source or in the coronal temperature. Details of the other coronal parameters are given in the text.



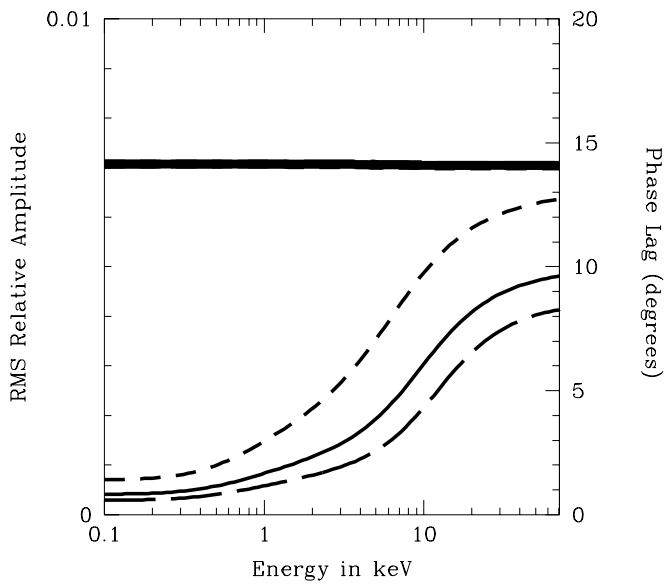
2a:  $\nu$ -dependence



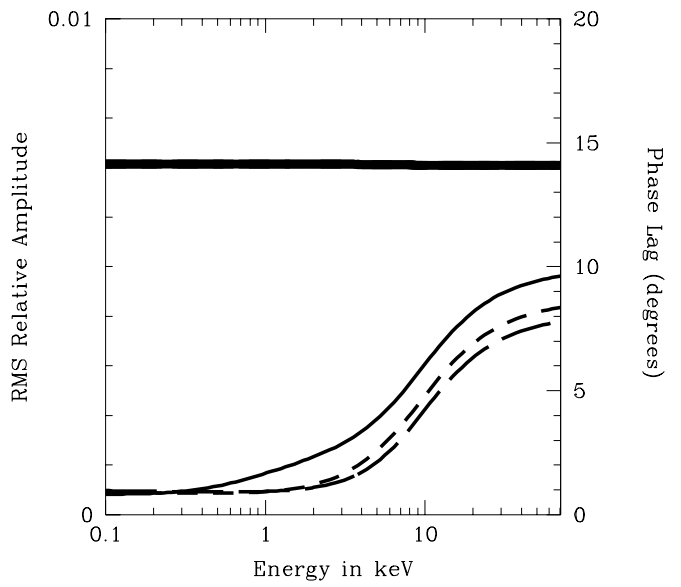
2b:  $\tau$ -dependence



2c:  $T_0$ -dependence

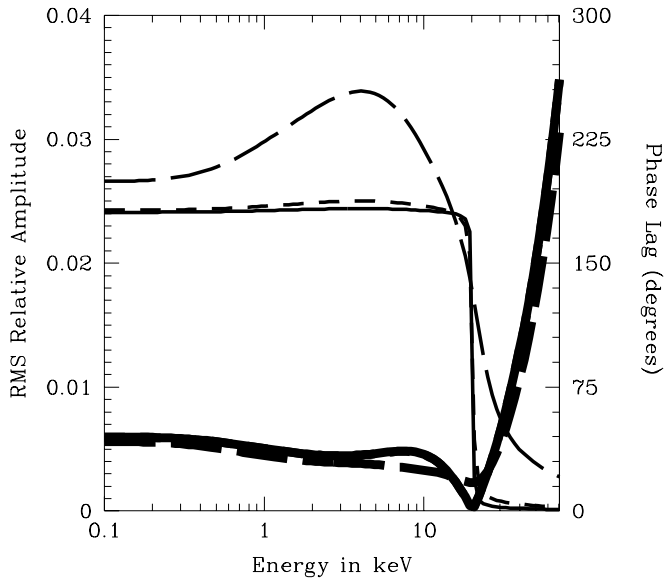


2d:  $T_{inj}$ -dependence

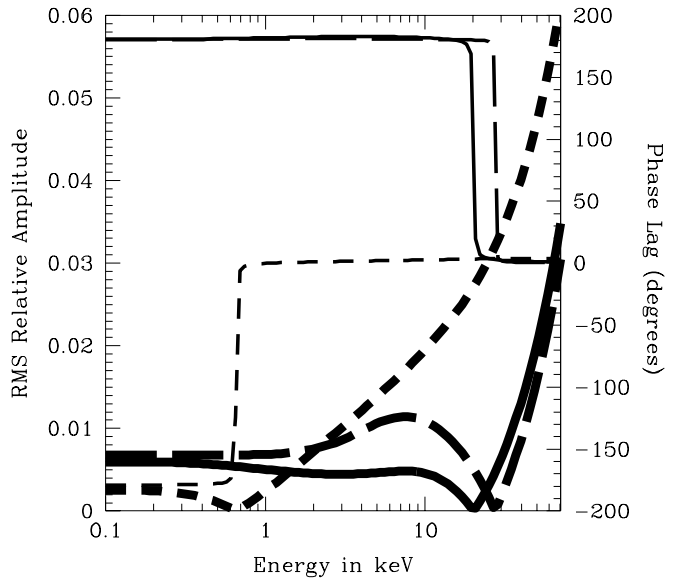




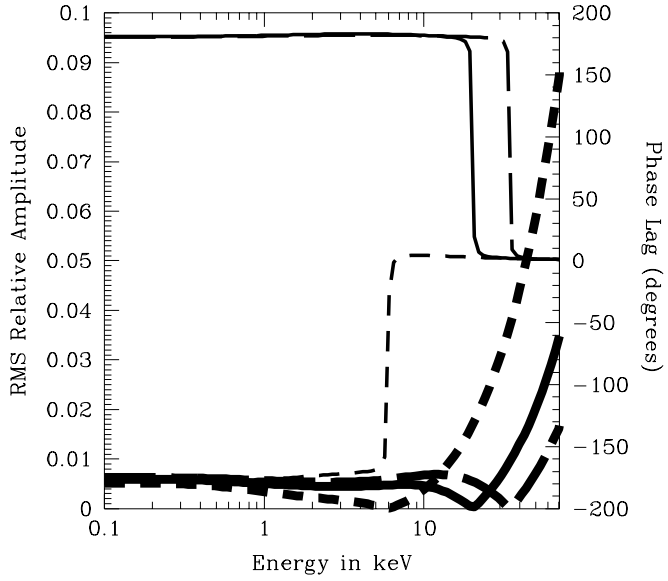
3a:  $\nu$ -dependence



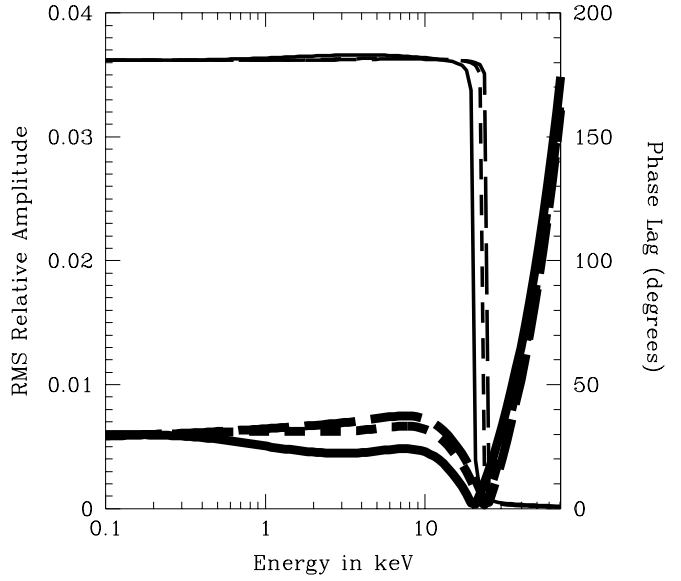
3b:  $\tau$ -dependence



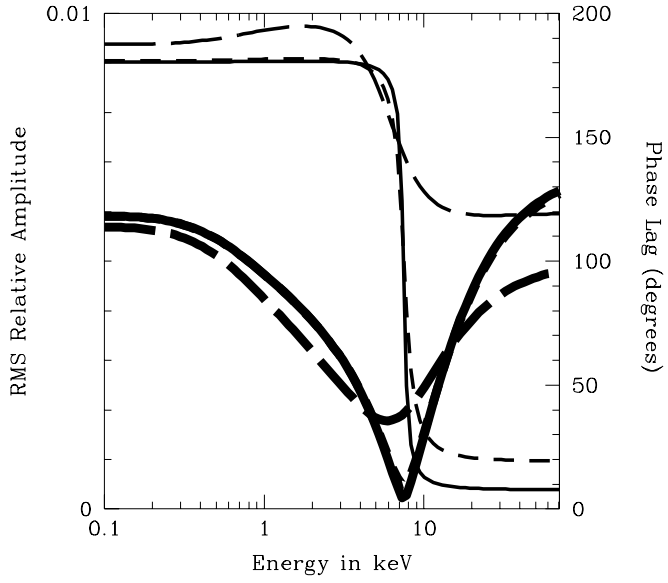
3c:  $T_0$ -dependence



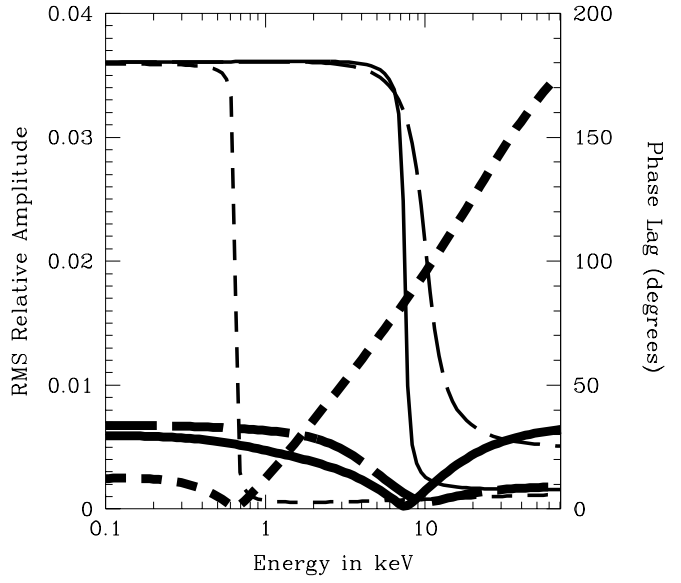
3d:  $T_{inj}$ -dependence



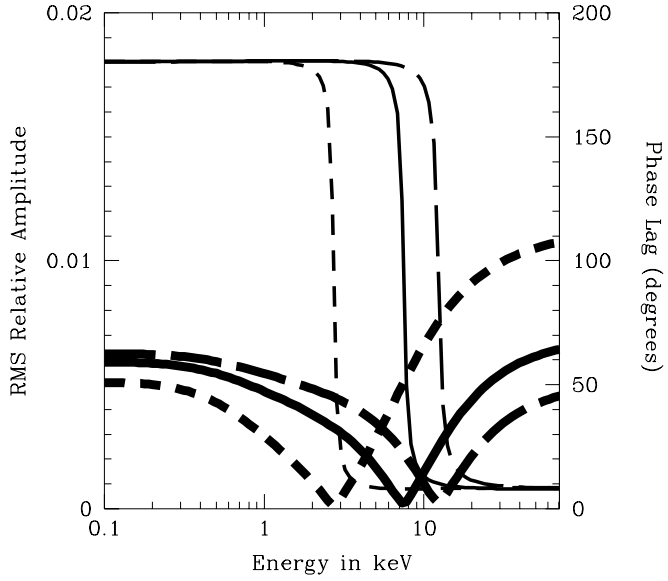
4a:  $\nu$ -dependence



4b:  $\tau$ -dependence



4c:  $T_0$ -dependence



4d:  $T_{inj}$ -dependence

